Chemical equilibrium and freeze-out in nuclear collisions at the CERN SPS

Masashi Kaneta

Department of Physics, Faculty of Science,
Hiroshima University,
Higashi-Hiroshima 739, Japan

February 14, 1996

Abstract

The temperature at freeze-out is given and the existence of transverse flow is indicated by transverse mass distribution of positive and negative π, K and p and $\bar{p}$ around central rapidity region from NA44 experiment at Pb+Pb collisions of CERN SPS. The baryon and strangeness chemical potential are given by the ratio K^-/K^+ and $\bar{p}/p$, and some thermodynamical variables are calculated at freeze-out. The energy density and baryon density at formation time is estimated and a result suggests that there is a possibility of QGP phase in Pb+Pb collisions at CERN SPS.

Contents

1 Introduction

1.1 Quark-Gluon Plasma

The prediction of QCD is saying that *quark-gluon plasma* (QGP) exists under high temperature and high pressure. This state is expected in the early universe, at the inside of neutron star and in the high energy nucleus-nucleus collisions. Fig. 1 shows the phase diagram for Hadron gas and QGP. We can experiment only the

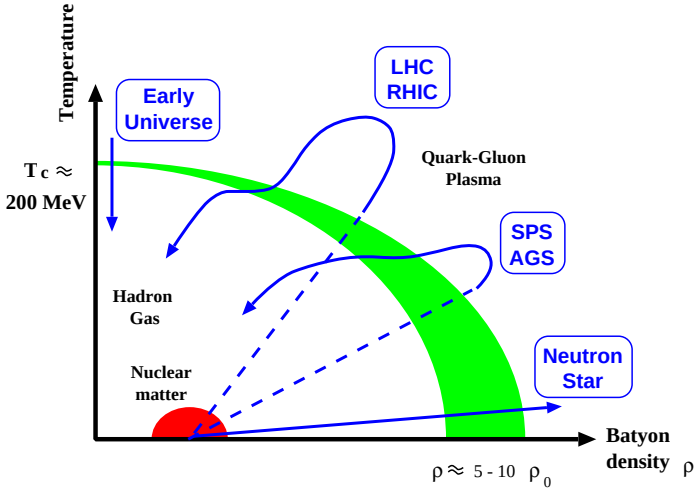

Fig. 1. Phase diagram for Hadron gas and QGP

third with accelerator on the earth. Some experiments have been executing to find the signal of QGP at CERN[1,2] (European Laboratory for Particle Physics) and BNL[3] (Brookhaven National Laboratory) since 1980's.

The following phenomena are expected as the signal of QGP.

- J/ψ suppression
- strangeness enhancement
- direct photons from collisions and excess of lepton pairs
- large size and long life source of particle
- temperature and hadrochemistry.

[1]The acronym CERN comes from the earlier French title: "Conseil Européen pour la Recherche Nucléaire"

[2]`http://www.cern.ch/`

[3]`http://www.bnl.gov/bnl.html`

The experiment related with QGP search has been studying and a current experiment at CERN and BNL is called second generation. In the first generation, it is expected to be easy to find QGP. However, it had been understood that the signal of QGP is not clear. Then, at the second generation, experiments which is focused a few phenomena have been doing.

The scenario of phase transition in heavy ion collisions is expected as the following. At time $\tau \sim 1$ fm, a local thermal equilibrium state makes up and QGP may is cleated around central region of system. The system expands hydrodynamically and the temperature of system is decreasing with increasing the volume. The phase transition from QGP phase to hadron gas is broken out at critical time. The hadron plays a high temperature and high pressure gas (fire-ball) At time $\tau = \tau_f$, the collisions and interaction in hadron gas are stopped and the particle come out (its state is called freeze-out).

In this paper, we watched the temperature and chemical potential at freeze-out and analysed lead on lead data of CERN NA44 experiment.

1.2 The NA44 experiment

The NA44[4] is 44th experiment at Norse Area of CERN and using a focusing spectrometer for one and two particles. The purpose of NA44 experiment are study of space-time expansion and temperature at heavy ion collision with particle identification.

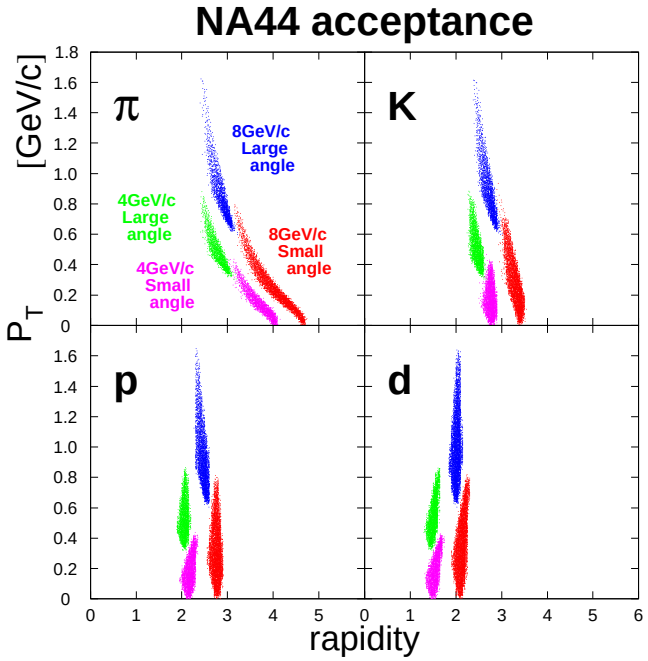

Fig. 2. Acceptance of NA44 experiment for π, K, p and d.

[4] http://p2hp2.lanl.gov/na44/na44.html

The feature are:

1. good momentum resolution ($\Delta P/P \simeq 0.2$ %)
2. good Time of Flight (TOF) resolution ($\simeq$ 100ps)
3. small acceptance around central rapidity region (see Fig.2)
4. and then possibility of particle identification of π, K, p and d

NA44 focusing spectrometer is upgraded to provide improved tracking and particle identification for lead beam from 1994. New detector are pad and strip chambers for tracking and aerogel cherenkov and multi-particle threshold imaging cherenkov. The description of set-up until sulfur beam is seen other papers [1, 2, 3].

Fig.3 shows NA44 spectrometer from 1994. The beam direction is left hand to right hand. Our spectrometer has 2 angle setting, 44mrad and 131mrad. This spectrometer consists of some magnets and detectors.

The cherenkov beam counter (CX counter) and the beam veto counter are used for definition of beam. CX counter defines start timing and has 35ps TOF resolution [4].

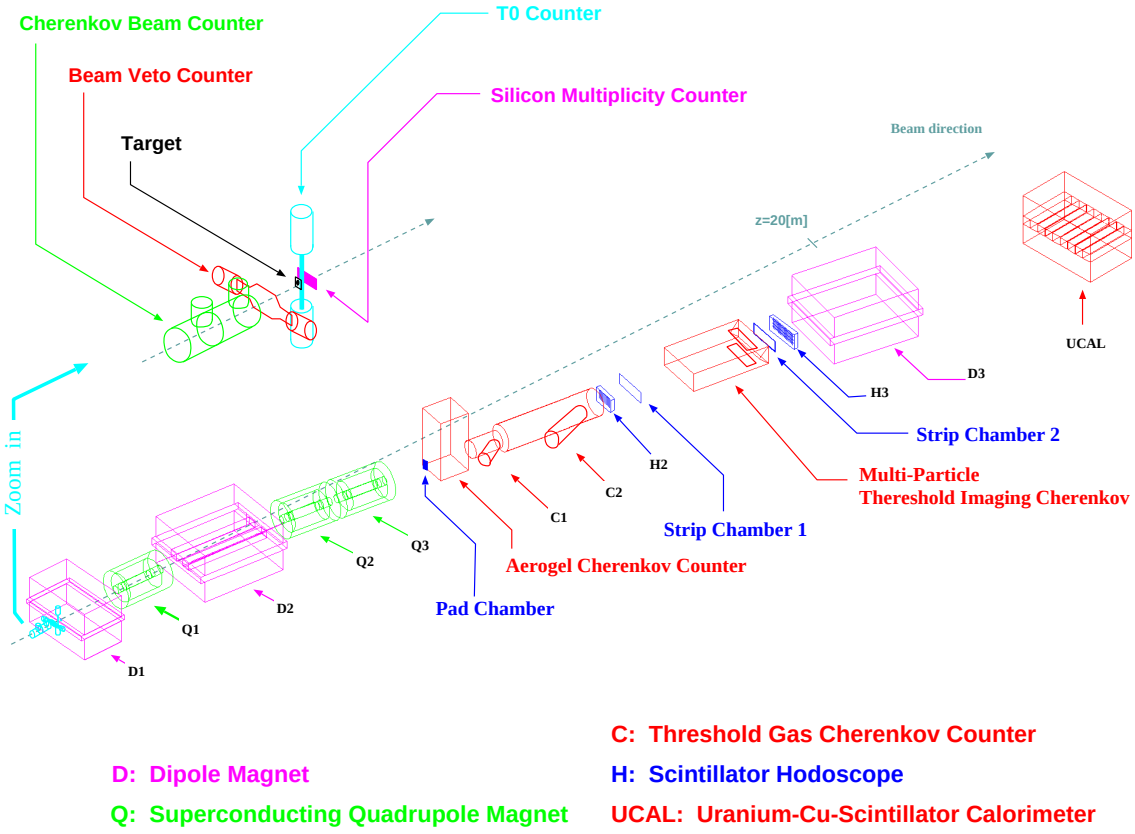

Fig. 3. NA44 set-up for lead beam (1994)

T0 counter and silicon multiplicity counter are used for definition of central collision. T0 counter consists of scintillator and two PMT. Silicon detector which consists of 512 pads is covered backward rapidity region.

The dipole magnets (D1 and D2) bend secondary particles and lead them to detectors at lower stream. This magnet is used for selection of momentum.

The super-conducting quadruple magnets (Q1 and Q2) focus secondary particles. By the changing focusing direction, we can change acceptance at the same angle and momentum region.

Pad chamber, two strip chambers and two hodoscopes (H2 and H3) are used for tracking and then these detectors is called as tracking detectors.

The particle species are identified by aerogel cherenkov counter, threshold gas cherenkov counters (C1 and C2), multi-particle threshold imaging cherenkov (TIC) and Uranium-Cu-scintillator calorimeter (UCAL).

1.3 A purely thermal source and chemical equilibrium

Assuming thermal and chemical equilibrium system [5] with temperature T, the invariant momentum spectrum is

$$E\frac{d^3N}{dp^3} = \frac{d^3N}{dy\, m_T\, dm_T\, d\phi} = \frac{gV}{(2\pi)^3} E e^{-(E-\mu)/T}, \tag{1}$$

where g is the spin-isospin degeneracy factor for the particle species, m_T is transverse mass: $m_T = \sqrt{m^2 + {p_T}^2}$ and μ is the chemical potential:

$$\mu = B\mu_B + s\mu_s \tag{2}$$

as originating from its baryon and strangeness quantum number B and s. The light (u and d) quark chemical potential is assumed to be same: $\mu_u = \mu_d \equiv \frac{1}{3}\mu_B$. Also $\hbar = c = k_B = 1$.

Under $m_T \gg m_T$ and narrow region of rapidity,

$$\frac{d^3N}{dy\, m_T\, dm_T\, d\phi} = V' e^{-(m_T-\mu)/T}. \tag{3}$$

The parameters of this distribution are the temperature T and the chemical potential μ_i. Eq.3 means that we can know the temperature from the m_T distribution of experiment to fit it $e^{-m_T/T}$. dN/dy is given by integrating Eq.3 over m_T and ϕ. The ratio of dn/dy between hadron and anti-hadron leads the chemical potential, directly. The ratio of $\bar{p}$ to p and K^- to K^+ are described as the following.

$$R_{K^-/K^+} = e^{-(\frac{2}{3}\mu_B + 2\mu_s)/T} \tag{4}$$

$$R_{\bar{p}/p} = e^{-2\mu_B/T} \tag{5}$$

We can calculate μ_B and μ_s from these equations.

In the nuclear, the strange-particle is very few, thus the strangeness from nuclear collisions almost comes from pair creation and total number of strangeness is zero.

In high density of particle, the energy to create $q\bar{q}$ must be the order of μ_q by Pauli principle but this limit is not valid for $s\bar{s}$. Then, in $\mu_q > m_s$, the creation of $s\bar{s}$ is more easy than $q\bar{q}$. The increase of strangeness occurs in QGP and also Hadronic-gas (HG). In HG, there is high density nucleon. The nucleon exchange s quark with K^- and changes to strangeness and hence the requirement of strangeness conservation normally leads to a considerable value of $\mu_s^{HG} \neq 0$. On the other hand, since in the de-confined QGP state both s and $\bar{s}$ quark are free, one always has $\mu_s^{QGP} = 0$.

The experiment measuring hadron sees some physical values after freeze-out, then it is not clear to get signal of QGP directly. However, some suggestion is given to us.

2 Analysis

2.1 Centrality

Centrality characterises the collisions and related impact parameter which is the distance between centres of beam and target nucleus. NA44 experiment uses a ratio, total number of secondary charged particles in central collisions to minimum bias collisions as centrality.

T0 counter is down-stream of target and counts charged particle. Minimum bias collisions event is measured without requiring T0 pulse height in trigger. Central collisions event measured with requiring high pulse height in trigger and/or off-line analysis.

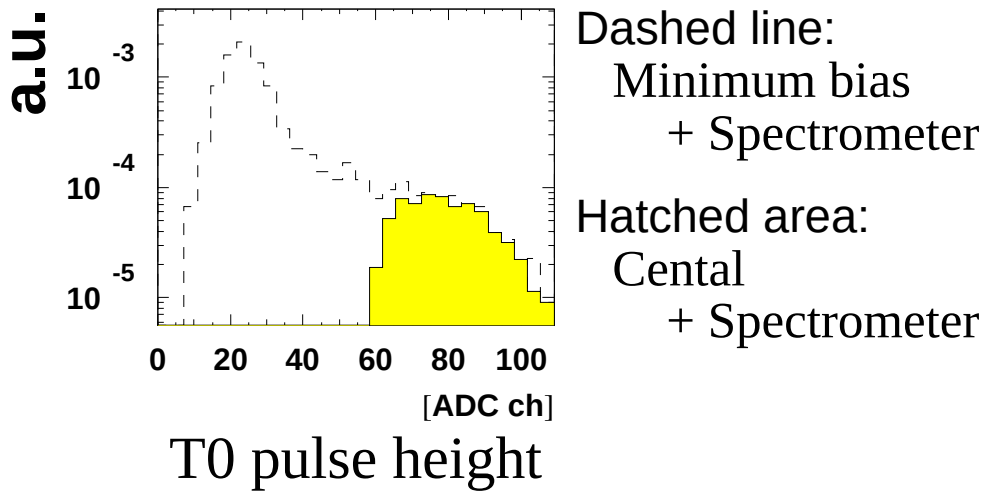

Fig. 4. Centrality measured with T0 counter

In Fig.4, the area described dashed line is T0 ADC distribution and no hatched area shows central event with requiring high pulse height of T0 in trigger. Two figures are normalised to overlap both spectrum shoulder. Centrality is calculated as ratio, hatched area to area described dashed line. In case of this figure, centrality is about 10%. We can get higher central event with higher T0 pulse hight.

The centrality of event used in analysis of this paper is 8%.

2.2 Particle identification

The pulse height of threshold cherenkov counters (C1, C2) and a mass square calculated by TOF and momentum are used for particle identification (PID).

The pressure of radiation gas of C1 and C2 are variable to set the threshold, respectively. We can select particle by on-line trigger and/or at off-line analysis from information of C1 and C2.

The track of particle is re-constructed from the information of hit on tracking detectors and give momentum. TOF for each track is calculated as the difference of TDC between the start counter (CX) and hodoscope, which has 60 (H2) or 50 (H3) slats and can define TOF slat by slat, respectively. This TOF is described as the following.

$$TOF = TOF_{peak} + \Delta TOF \tag{6}$$

This has a offset come from detector system and has a width of resolution. On the other hands, a primary particle is around this peak position and then β is described as the following,

$$\begin{aligned} \frac{1}{\beta} &= \frac{c\left((TOF_{peak} - TOF_{offset}) + \Delta TOF\right)}{L_{path}} \\ &= \frac{\sqrt{m_{prim}^2 + p^2}}{p} + \frac{c\,\Delta TOF}{L_{path}} \end{aligned} \tag{7}$$

where c is speed of light in vacuum, L_{path} is path length from target to slat of hodoscope, m_{prim} is rest mass of primary particle and p is absolute value of momentum of each track. From $1/\beta$ and p, mass square m_{ex} is described.

$$m_{ex}^2 = \frac{1-\beta^2}{\beta^2} p^2 \tag{8}$$

Fig.5 shows scatter plot of pulse height of C1 and C2, and mass square distribution at 4GeV setting.

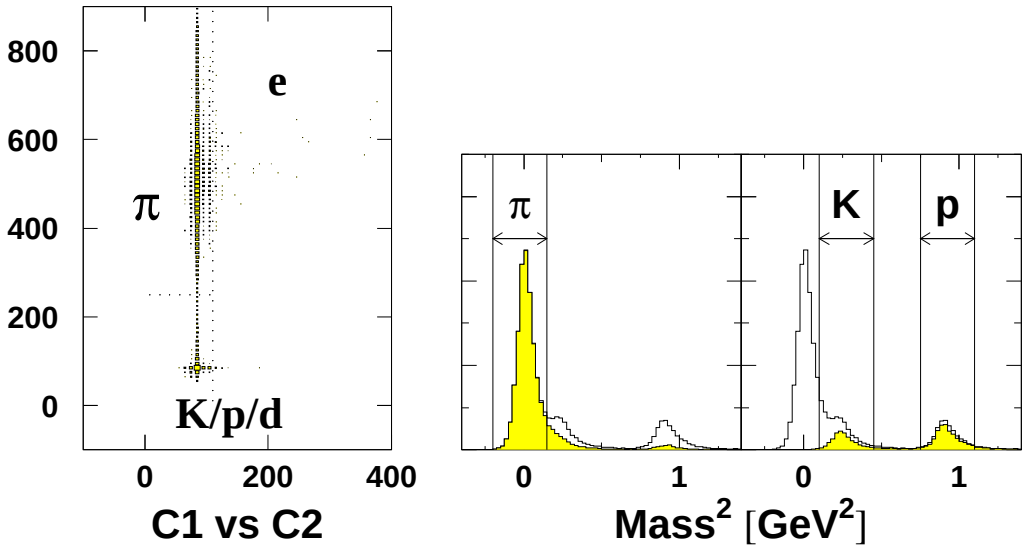

Fig. 5. Particle identification at 4GeV setting, unit of plot of C1 vs C2 is channel of ADC

The pedestal of C1 and C2 is not subtracted in this figure. Electron and pion fire photon at C1 and electron also fire at C2. In Fig.5, no hatched area of mass square distribution is required C2 pedestal to reject electron. Hatched area in left hand is required of C1 pulse height and one in right hand is not done. Pion, kaon and proton are selected like as figure.

TOF resolution at 8GeV setting is worse than at 4GeV setting. In this setting, the pressure of C1 and C2 are changed to high, then kaon fires at C1 and pion fires at C2. Since there is difference of mass between pion and kaon, the pulse hight of

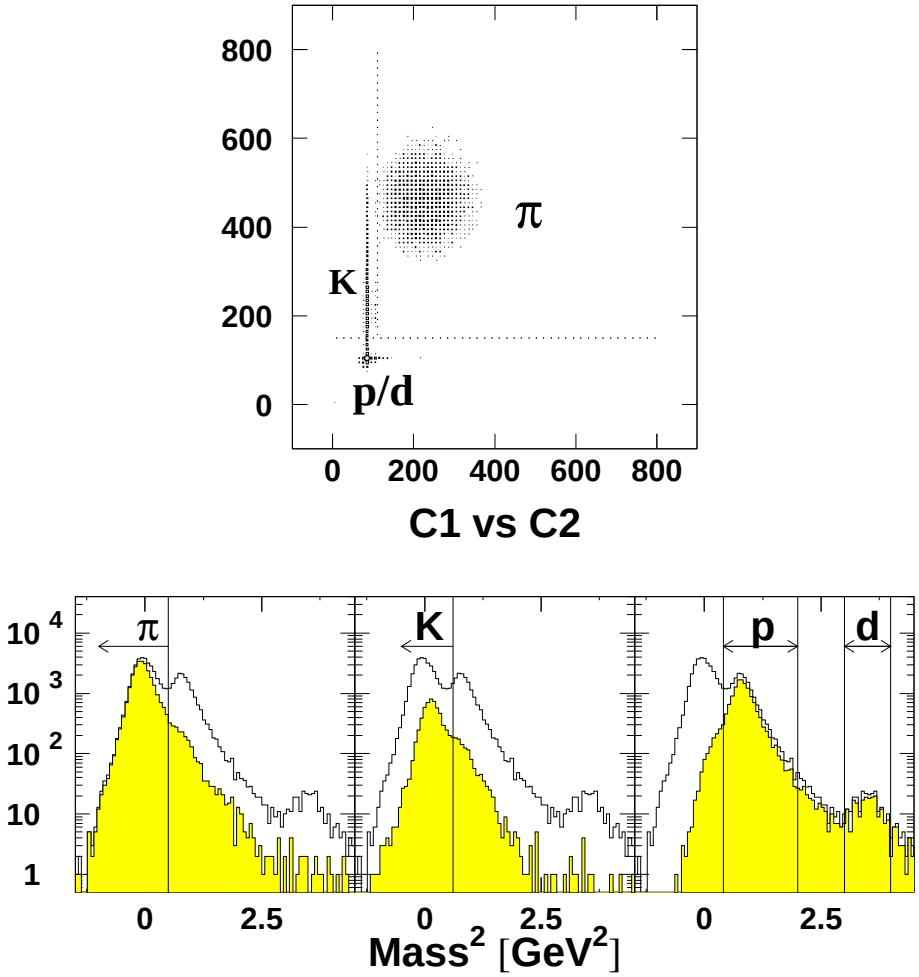

Fig. 6. Particle identification at 8GeV setting, unit of plot of C1 vs C2 is channel of ADC

C1 for kaon is lower than pion. The scatter plot of C1 and C2 in Fig.6 shows that difference with 4GeV setting. Three Mass square distribution is given by selecting reason in scatter plot. No hatched area is without cut of C1 and C2. Hatched area is candidate of pion, kaon and proton/deuteron. We can see contamination of kaon

and proton for pion candidate, proton for kaon and kaon for proton. Pion, kaon, proton and deuteron is selected from mass square shown by line in Fig.6.

In both setting, some tracks is rejected to get high purity. The number of rejected track is estimated by fit a function of mass square to count number of particle. The ratio, number of estimated track over selected track will be multiplied when calculating cross-section. This ratio is called cherenkov veto factor.

2.3 Acceptance correction

Since spectrometer affects a distribution of physical values measured, this acceptance have to be corrected to get an original distribution. To correct acceptance effect, Monte Carlo simulation is used. In the simulation, the event of collisions generate to follow an momentum spectrum assumed as the following.

$$\frac{d^3n}{dy\, m_T\, dm_T\, d\phi} \propto \exp\left(-\frac{m_T}{A}\right) \exp\left\{-\left(\frac{y-B}{2C}\right)^2\right\} \tag{9}$$

A is an inverse slope parameter of exponential function of m_T distribution. B is peak of Gaussian distribution as function of rapidity and C is width.

A acceptance correction factor for m_T distribution is given as the following step. The generated particles throw into NA44 acceptance and make hit on each detectors

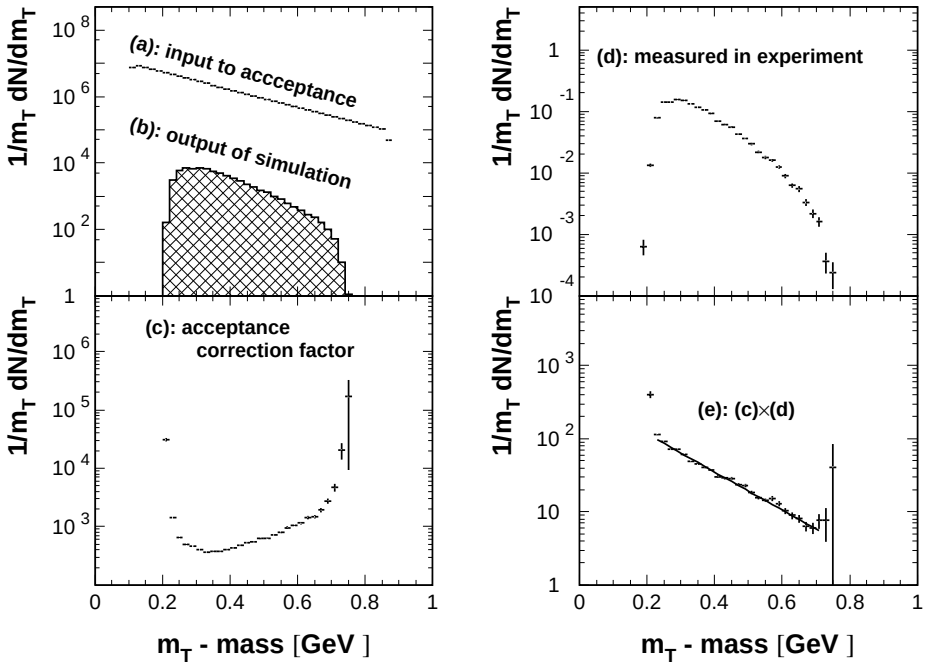

Fig. 7. Acceptance correcton. (a) is input to acceptance in simularion. (b) is output of simuration. (c) is acceptance correction factore given (a) diveded by (b). (d) is experimental distribution. (e) is distribution corrected acceptance effect given (d) mulplied (c). Solid line is fit by exponetial function.

in simulation. The track is reconstructed by a routine which is same one used for reconstructing experimental data. $1/m_T\, dn/dm_T$ distribution for input of simulation and output are given (Fig.7-(a),(b)). The acceptance correction factor is given (a) divided by (b) in Fig7. The effect of acceptance is correct by multiplying the acceptance correction factor to experimental $1/m_T\, dn/dm_T$ distribution (Fig.7-(e)).

Since the acceptance of NA44 experiment is narrow (see Fig.2), rapidity part of Eq.9 have to be refer dN/dy distribution from other experiment. In this analysis, the result of other experiment at CERN SPS is used.

2.4 Normalization

A normalization is need to get an absolute cross section per one collision. The normalization factor, F_{nor} is given as the following,

$$F_{nor} = \frac{1}{N_{beam}\,\sigma_{int}\,\sigma_{trig}} \frac{N_{pre}}{N_{acc}}\, F_{cv} \tag{10}$$

where N_{beam} is number of beam particles during data taking, σ_{int} is geometrical interaction probability, then $N_{beam}\,\sigma_{int}$ means minimum bias collision, σ_{trig} is trigger centrality (see sub-section 2.1), therefore $N_{beam}\,\sigma_{trig}\,\sigma_{int}$ is number of minimum bias collision, N_{pre} is number of presented trigger, N_{acc} is number of accepted trigger, so N_{pre}/N_{acc} corrects dead time by DAQ and F_{cv} is cherenkov veto factor explained in sub-section 2.2 and estimated for each particle species.

The absolute cross section per event is,

$$\frac{1}{N_{event}} \frac{d^3n}{dy\, m_T\, dm_T\, d\phi} = F_{nor}\, \frac{1}{2\pi} \frac{\Delta n}{\Delta y} \frac{dn}{m_T\, dm_T} \tag{11}$$

where the factor $1/2\pi$ is given by assuming uniformity of collisions for ϕ direction, $\Delta n/\Delta y\; dn/m_T dm_T$ is corrected acceptance effect for experimental data.

After absolute cross section is given, dN/dy can be calculated. The distribution described by Eq.11 is fit a function of K_T ($K_T = m_T - mass$),

$$\frac{1}{N_{event}} \frac{d^3n}{dy\, m_T\, dm_T\, d\phi} = f(K_T) \tag{12}$$

and dN/dy is given by integrating as the following,

$$\frac{dN}{dy} = 2\pi \int dK_T\; m_T f(K_T) \tag{13}$$

When $f(K_T)$ is $\mathrm{A}\exp(-K_T/\mathrm{B})$, Eq.13 is described as

$$\frac{dN}{dy} = 2\pi \mathrm{AB}\,(m + \mathrm{B})\,, \tag{14}$$

where A and B are fitting parameter and m is rest mass of the particle of the m_T distribution.

3 Results and Discussions

3.1 Transverse mass spectrum from Pb+Pb

After normalization, we get the m_T distribution. Fig.8 shows cross section as function of $K_T(= m_T - mass)$ for each particle around central rapidity region $y = 3 \sim 4$. The horizontal axis is shifted by subscripting mass of each particle from m_T to adjust start point of the distribution for all particle). The top figure shows the production cross section as function of K_T for positive charged pion and kaon and proton. The bottom shows the distribution for negative charged pion and kaon and anti-proton. Since there are enhancement around low K_T and excess around high K_T, it is no good for the pion distributions to fit single exponential as function of K_T over all range (from 0 to 1.5 GeV).

For the enhancement around low K_T, one of candidate of this effect is decay of resonance. For the resonance effect, please see the reference [3]. We fit the pion distributions by single exponential function from 0.3 GeV to 1.0 GeV to compare the inverse slope with kaon and proton. On the other hand, for the distributions of kaon and proton/anti-proton, fitting by single exponential function of K_T looks good.

Some points to note about K_t distribution are the following. The inverse slope is same in errors region between π^+/π^-, K^+/K^- and $p/\bar{p}$, respectively. On the other hand, it is different between pion, kaon and proton. This means inverse slope depends on rest mass of particle. The dependence of mass for inverse slope parameter is summarized in Fig.9. The p+p from ISR and NA44 S+S data is put on Fig.9 to compare with Pb+Pb data to see the difference of colliding system.

As stated in sub-section 1.3, the inverse slope parameter shows a temperature of source on assuming thermal equilibrium and Eq.3 explains that the inverse slope parameter has independence of mass. However, there is the discrepancy between purely thermal equilibrium model and the results of experiment about the *temperature*. We can see that the value of inverse slope is increasing with lager mass of particle and this effect is stronger with larger system of collisions. The increasing of inverse slope parameter suggests that there is a hydrodynamical flow in the thermal equilibrium source.

In the first order approximation, there is a relation between measured inverse slope T_m, freeze-out temperature T_f and rest mass M [12]. It is

$$T_m = T_f + \frac{1}{2}\beta_s^2 M, \tag{15}$$

where β_S is a hydrodynamical surface flow velocity. To fit this formula for S+S and Pb+Pb data in the By fitting Eq.15 to the data point in Fig.9 with systematic errors, the freeze-out temperature is given 150 to 170 MeV around central rapidity region in the nuclear collisions at the CERN SPS energy. And the experimental results suggest the stronger flow effect with increasing colliding system.

Let's think a limit of the freeze-out temperature. If the temperature of system is higher than pion mass, a part of energy may use for pion creation and temperature is

decrease until stopping pion creation. Since freeze-out is a state which the reaction and particle creation in the system is stopped, the freeze-out temperature may be less than 140 MeV. However, the result of fitting by Eq.15 is higher than pion mass.

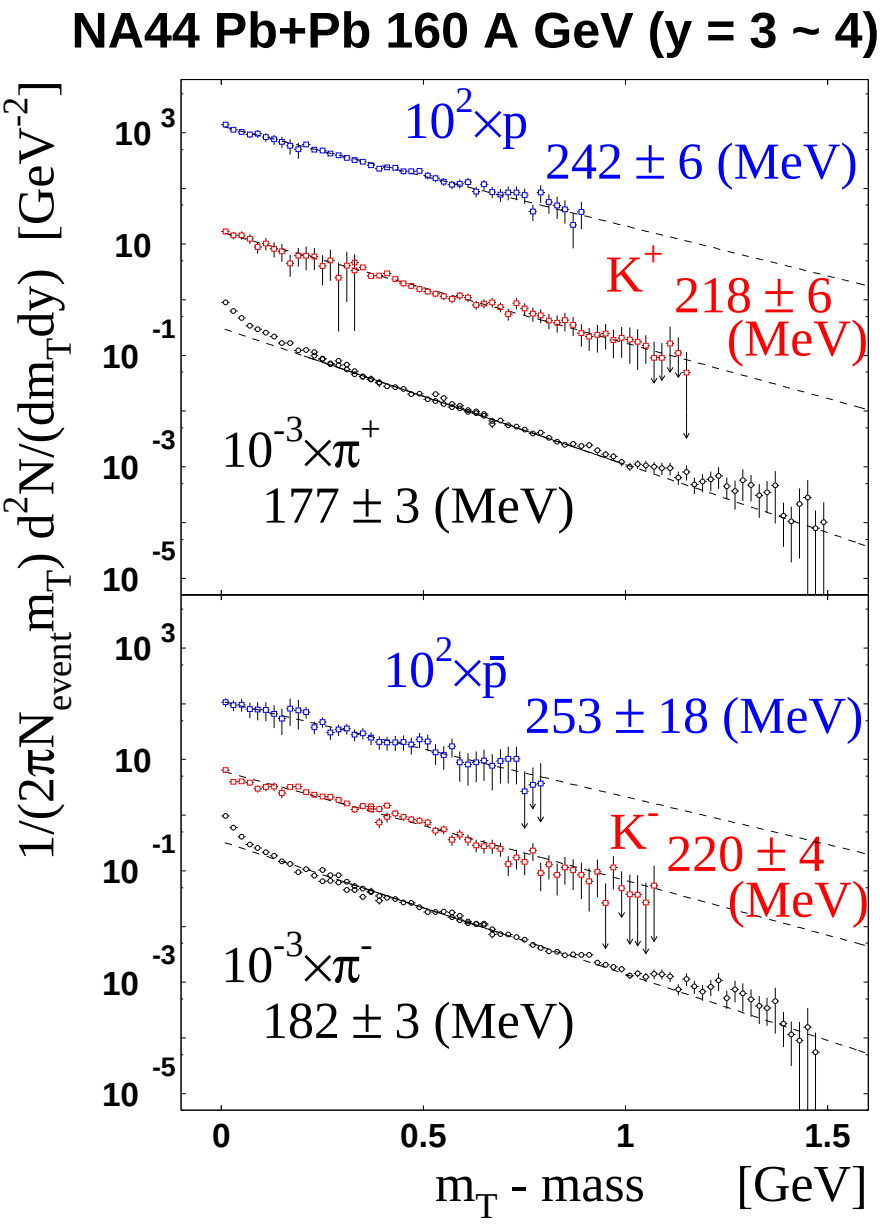

Fig. 8. $K_T (= m_T - mass)$ distribution for positive and negative particle. Top shows positive particles and bottom shows negative particles. The values close to slope is inverse slope parameter on fitting the distribution by $A \exp(-K_T/B)$. For pion, fitting range is 0.3 to 1.0 [GeV]. For the other particle, fitting is done for all point on figure.

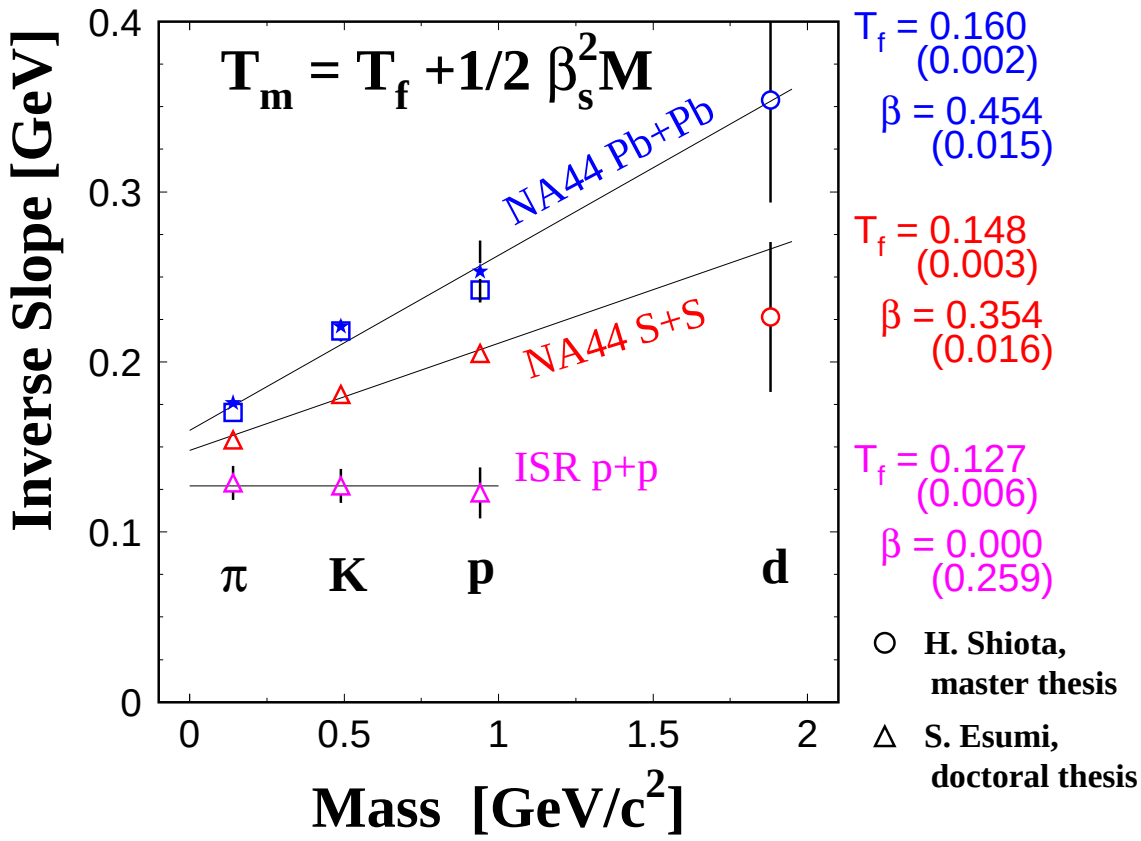

Fig. 9. Summary of inverse slope parameters. Solid character show negative charged particle. Open character shows positive charged particle. Solid star and open square come from Fig.8. Open circle comes from S. Shiota's master thesis [6]. Open triangle comes from S. Esumi's doctoral thesis [3].

3.2 Comparison with hydrodynamical model calculation

In this sub-section, we compare with hydrodynamical model in detail. There are some papers [5, 7, 8] which tested thermodynamic model and hydrodynamical model. These show a hydrodynamical model describes well the $1/m_T\ dN/dm_T$ distributions for different particle by only two parameters, the freeze-out temperature T_f and the surface velocity of flow β_s [5, 8].

We describe the transverse velocity distribution $\beta_r(r)$ by β_s and parameterized in the region $0 \leq r \leq R$.

$$\beta_r(r) = \beta_s \left(\frac{r}{R}\right)^n, \tag{16}$$

where R is a radius of the thermal source at freeze-out. With n we can vary the form of the profile but the form of the profile is not important for the analysis. We have used $n = 1$ in the subsequent calculations.

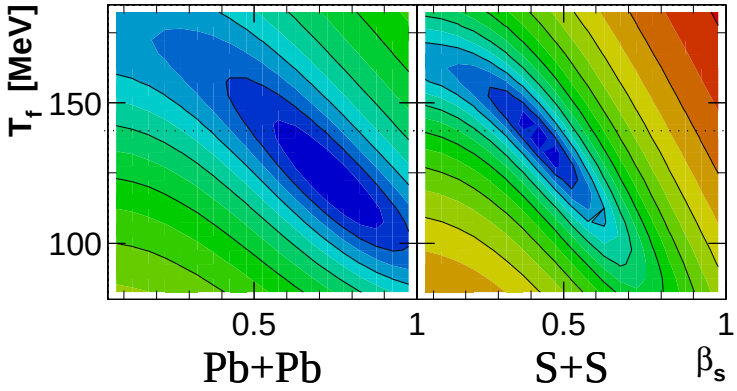

Fig. 10. The contour plot of χ^2 map for fitting of hydro-dynamical model calculation for $1/m_T\, dN/dm_T$ spectra. The horizontal dot line is on $T_f = 140$ MeV which is Hagedorn limit of freeze-out temperature. The solid contour lines designate the area of $\chi^2/NDF = \chi^2_{min}/NDF+$ 1, 2, 4, 8, 16, 32 and 64.

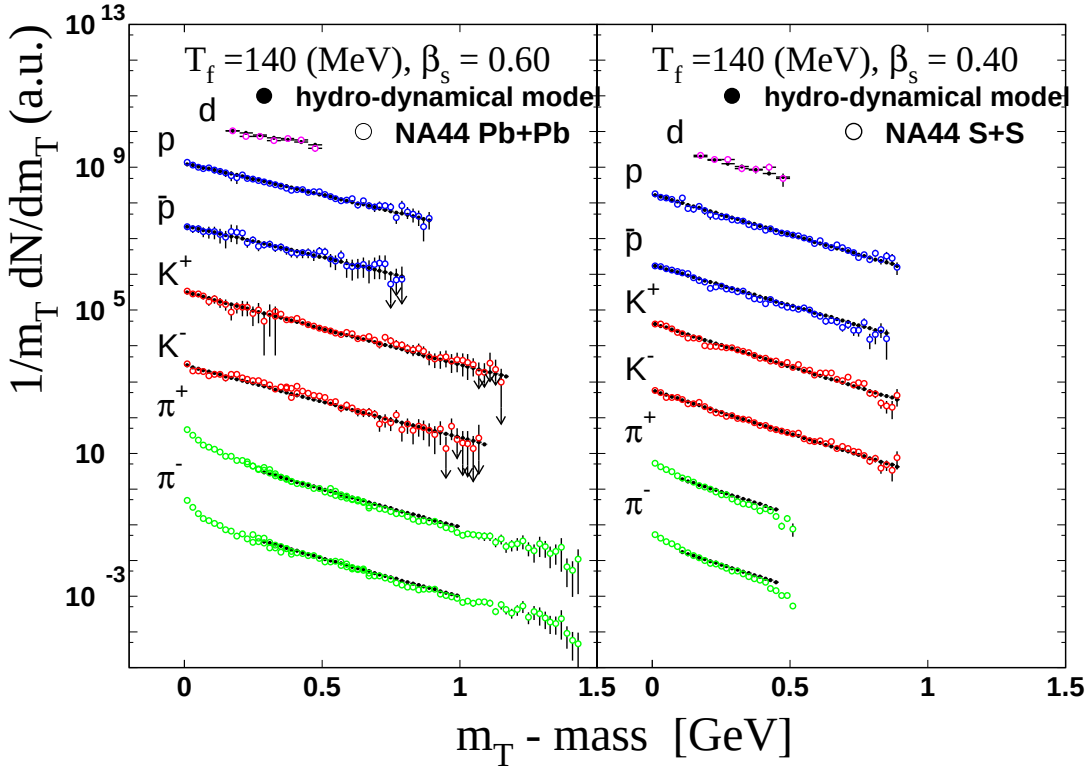

Fig. 11. Fitting hydro-dynamical calculation to transverse mass spectrum for NA44 Pb+Pb and S+S data. The spectra of $\pi, K, p/\bar{p}$ in left side come from Fig.8. The spectra of $\pi, K, p/\bar{p}$ in right side are preliminary data. For deuteron in both figure came from H. Shiota's master thesis [6].

Assuming that the longitudinal and transverse motion of the thermal source are decoupled, flow effects can be incorporated into transverse mass spectra as the following.

$$\frac{dN}{m_T\, dm_T} \propto \int_0^R dr\, r\, m_T\, I_0\left(\frac{p_T \sinh\rho}{T_f}\right) K_1\left(\frac{m_T \cosh\rho}{T_f}\right), \qquad (17)$$

where ρ is the boost angle and $\rho = \tanh^{-1}\beta_r$.

We calculated Eq.17 for pion, kaon, proton and deuteron in the region from T_f = 80 MeV to 180 MeV with every 5 MeV and β_s = 0.05 to 0.95 with every 0.05. The calculated spectrum is fit for experimental data for each particle and we got a χ^2 map for fitting as Fig.10. For comparison between colliding systems, Fig.10 has two maps which are result of fitting for Pb+Pb and S+S from NA44 experiment. The result of fitting shows T_f = 100$\sim$160 MeV and β_s=0.4$\sim$1.0 for Pb+Pb and T_f = 120$\sim$160 MeV and β_s=0.3$\sim$0.6 for S+S. We estimate the freeze-out temperature is 140$\pm$ MeV from the previous results and this results. At T_f = 140 MeV, $\beta_s = 0.50 \sim 0.70$ for Pb+Pb and $\beta_s = 0.35 \sim 0.45$ for S+S. This suggests that there is stronger transverse flow with larger colliding system at same freeze-out temperature.

It looks good to fit the transverse mass spectrum for some particles by hydrodynamical model calculation in Fig.11.

3.3 Chemical potential

To calculate chemical potential, we have to get the particle production ratio, K^-/K^+ and $\bar{p}/p$. At first, we calculated dN/dy of each particle from normalized production cross section which is shown in Fig.8. As said in sub-section 3.1, single exponential function of m_T can not describe the pion spectrum for Pb+Pb data. To fit the pion spectrum, $A\exp(-K_T/B) + C\exp(-K_T/D)$ is used as fitting function for instant calculation of dN/dy. The value of dN/dy for each particle is shown in Fig.12.

For the positive and negative pion, the values of dN/dy of both is same. This is sufficient condition for the assumption that the chemical potential of u and d quark is same.

The ratio K^-/K^+ and $\bar{p}/p$ is summarized in the Fig.13 to compare with other colliding system[17]. The both ratio is decreasing with increasing colliding system. This suggests the potential is increasing if freeze-out temperature is same for p+S, S+S and Pb+Pb.

Fig.14 shows scatter plot of the baryon chemical potential μ_B and the strangeness chemical potential μ_s. μ_B is calculated Eq.5. μ_s is calculated Eq.4 and μ_B. To check consistency of values, the point calculated from $\bar{\Lambda}/\Lambda$ and $\bar{p}/p$ are put for p+S and S+S. The two values of strangeness chemical potential from p+S has not so good agreement. This may mean that the assumption of chemical equilibrium is not satisfied in p+S collisions. For S+S data, It has good agreement.

S+S and Pb+Pb data looks $\mu_s \simeq 0$, then we assumed $\mu_s = 0$ for S+S and Pb+Pb data and the values of μ_B is shown in Fig.15. The average of μ_B is 147 $\pm$ 17 MeV for S+S and 184 $\pm$ 24 MeV for Pb+Pb. The chemical potential and temperature is given, then we can get some thermodynamical variables at the freeze-out. To

get some variable, we need to treat the system as thermal equilibrium only after the initially hot and dense fireball has expanded and reached the freeze-out density. Therefore, the system described by a grand canonical ensemble of non-interacting fermions and bosons (free gas of hadron) in equilibrium at freeze-out temperature T_f.

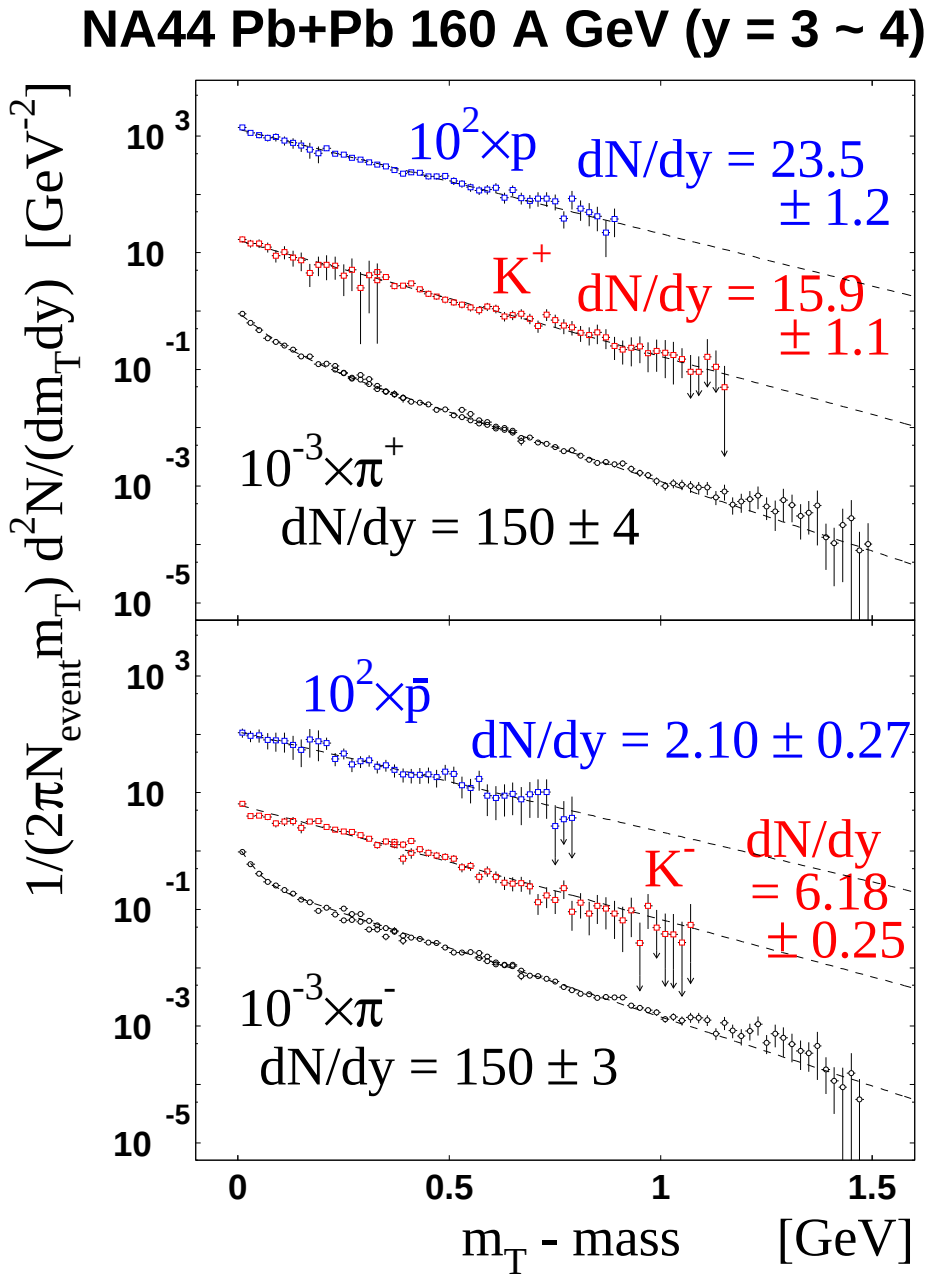

Fig. 12. The result of fitting and dN/dy of each particle. For pion, $A\exp(-K_T/B) + C\exp(-K_T/D)$ is used as fitting function. For kaon and proton/anti-proton, $A\exp(-K_T/B)$ is used. The way of calculation of dN/dy is indicated in sub-section 2.4.

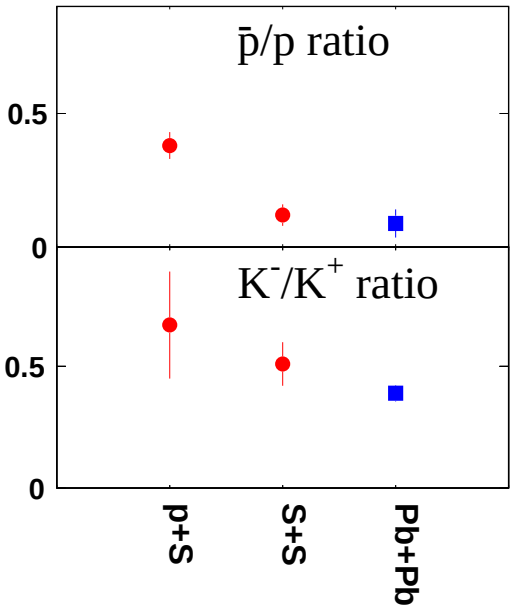

Fig. 13. Comparison the ratio of K^-/K^+ and $\bar{p}/p$ with other experiment. p+S data and S+S data come from reffernce [17]

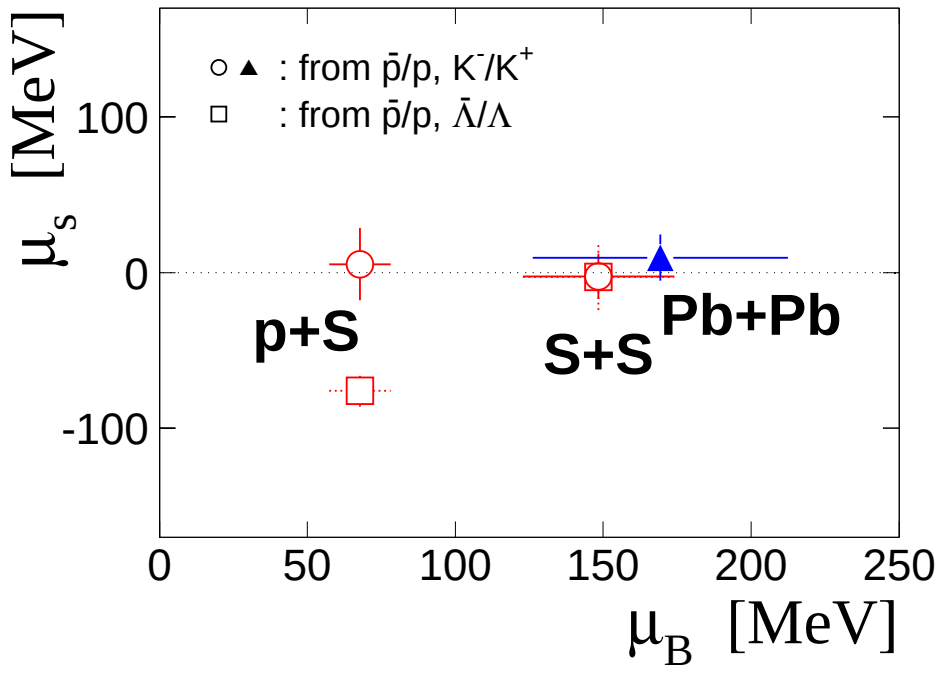

Fig. 14. Scatter plot of baryon and strengeness chemical potential. p+S data and S+S data come from reffernce [17] for $\bar{p}/p$ and [18] for $\bar{\Lambda}/\Lambda$ and

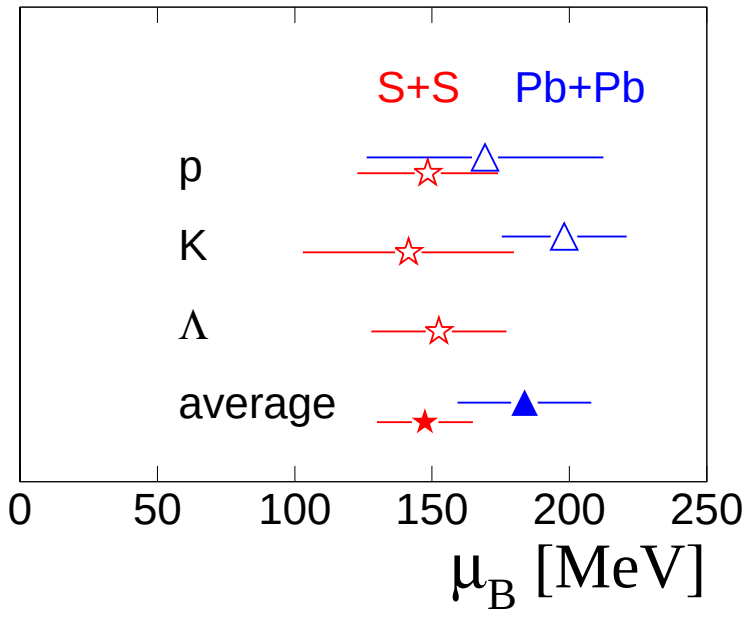

Fig. 15. μ_B calculated from each particle with assuming $\mu_s = 0$ (open character). Star is from S+S data. Triangle is Pb+Pb data. Solid character is average of μ_B for S+S and Pb+Pb, respectively.

We get the chemical potential and temperature, therefore, the thermodynamical potential is given and we can calculate some thermodynamical variables.

Baryon density ρ_i describe as the following.

$$\rho_i = \frac{g_i}{2\pi^2} \int \frac{p^2 dp}{\exp(E_i - (B_i\mu_B + s_i\mu_s)/T_f) + 1} \ , \tag{18}$$

where g_i is the spin-isospin degeneracy of particle i, E_i is its total energy in the local restframe, B_i and s are the baryon and strangeness quantum number and μ_B and μ_s is baryon and strangeness chemical potentials (also, $\hbar = c = k_B = 1$). Eq.18 is integrated over infinite space and then have to be multiplied [10] by a correction factor which we evaluate for a spherical volume with radius R. We also apply the excluded volume correction [7, 11, 16] to take into account the volume occupied by individual baryon with radii of 0.8 fm.

Fig.16 show phase diagrams for some thermodynamical variables. The top-left histograms shows the scatter plot of the temperature and baryon chemical potential. Solid triangle and star are Si+Au and Si+Pb data at AGS [9, 8]. The values of temperature, chemical potential and surface flow velocity are summarized in Table.1 A yellow belt on histograms is phase diagram come from reference [13]. Both data, AGS and CERN say the state of the freeze-out close to the phase boundary. The top-right histogram shows the scatter plot of the temperature and baryon density. The value of the baryon density from S+S and Pb+Pb collisions at CERN SPS are close

	T_f(MeV)	μ_B(MeV)	μ_s(MeV)	β_s
S+S	140±10	147±17	0	0.40±0.05
Pb+Pb	140±10	184±24	0	0.60±0.10
Si+Au	127± 8	485±70	68(+20,-16)	————
Si+Pb	130±10	540	121.5±13.5	0.54±0.04

Table 1. Summary of temperature, baryon and strangeness chemical potential and surface flow velocity.

to each other and smaller than the values from AGS data. The point to note is the baryon density at freeze-out is smaller than the nuclear matter density. This suggests the volume of system is larger than initial state (normal nuclear matter) or many nucleons are used making lighter particle than nucleon. The bottom histogram is the scatter plot of baryon density and energy density. Solid characters show the value at freeze-out. Open characters and dot line connecting between same characters shows minimum and maximum estimated point at formation time when hadron is cleated after collisions.

To estimate the values at formation time, we assumed that the fire-ball is ideal fluid and surface flow velocity equals the velocity of expanding fluid and used energy momentum tensor. At formation time, assuming that the fluid is stopping and the energy density ε and pressure p is uniform in the fluid from formation time t_0 to freeze-out time t_f, the energy density at t_0, $\varepsilon(t_0)$ is described as the following.

$$\varepsilon(t_0) = \frac{V_f}{V_0}\left(\varepsilon(t_f)\, u_0^2 + p(t_f)\, |\boldsymbol{u}|^2\right), \tag{19}$$

where $u_0^2 = 1/(1-\beta^2)$, $u_0^2 - |\boldsymbol{u}|^2 = 1$ and V_0 and V_f are the volume at t_0 and t_f. By same assuming, baryon density at t_f can be described.

$$\rho(t_0) = \frac{V_f}{V_0}\rho(t_f)\, u_0 \tag{20}$$

For the minimum estimate, we assumed $V_0 = V_f$. For the maximum estimate, we used simple model for the volume. At t_0, colliding system is like disk with thickness ~ 1 fm and radius $= R$, where $R = 1.2A^{1/3}$ and A is mass number of atom. Until t_f, we assumed that the system is expanding with light velocity c for the longitudinal direction and with surface velocity β for transverse direction, cylindrically. To this calculation, we also need to estimate freeze-out time. We used a freeze-out time which is estimated HBT analysis (two particle interferometer). Some recent analysis of HBT give us $4 \sim 5$ fm as freeze-out time in S+A collisions at CERN SPS[14, 15]. This value is close to the radius of sulfur $1.2A^{1/3} \sim 3.8$ fm. We applied the radius of Si, S, Pb as freeze-out time of Si+Pb, S+S and Pb+Pb collisions, respectively.

The ratio V_f/V_o is more sensitive to estimate baryon and energy density than effect of flow. We can see the maximum baryon density is about 3 times of nuclear matter for Si+Pb at AGS and same with nuclear matter for Pb+Pb. For energy

density, the estimated value at formation time in Pb+Pb collisions are overlapped a energy density at phase transition between QGP phase and hadron gas phase ($0.86 \sim 2.5$ GeV/fm^3).

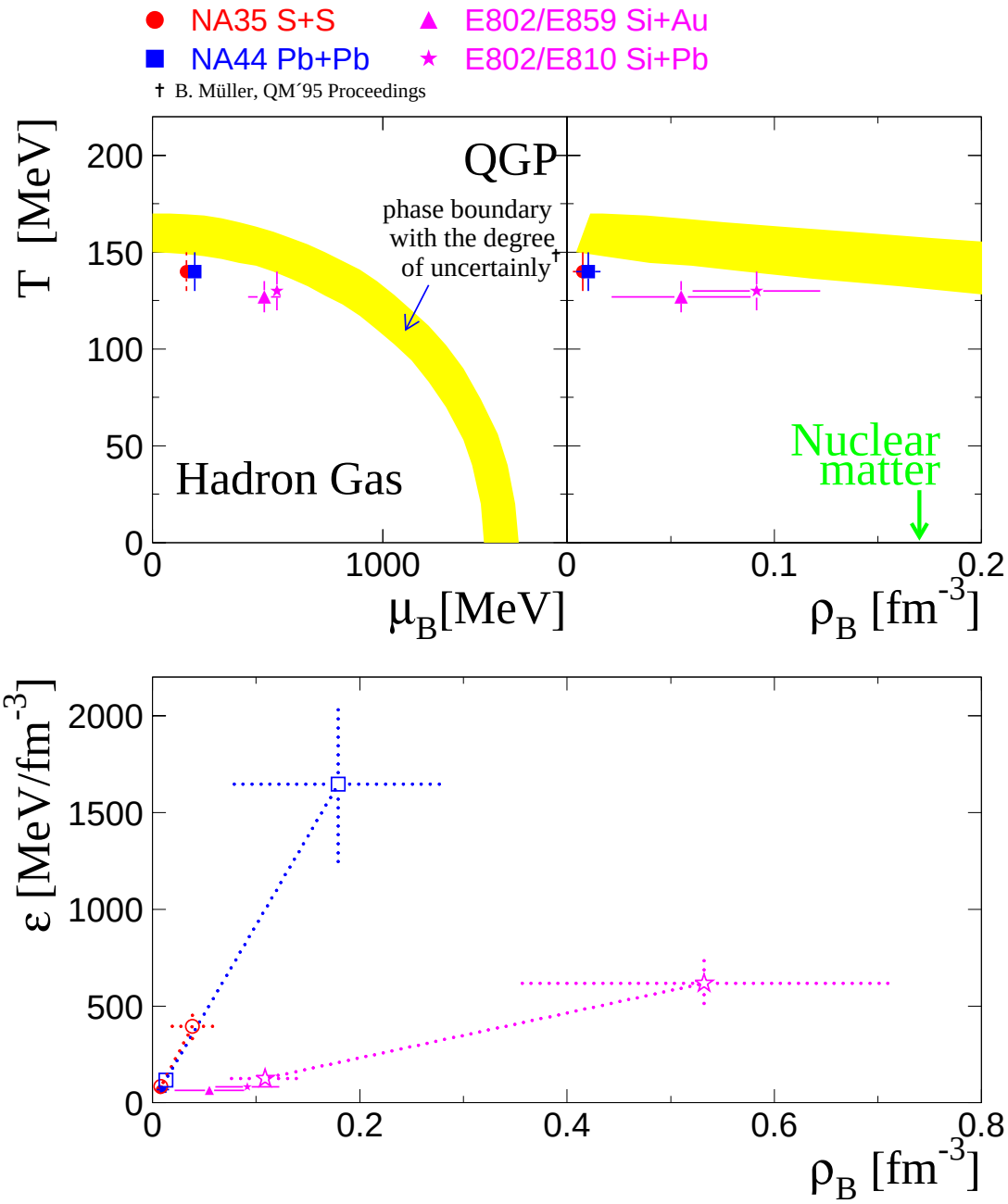

Fig. 16. Phase diagrams for S+S, Pb+Pb. For comparison, data of Si+Au and Si+Pb at AGS are on each histogram. T, μ_B, ρ_B and ε are temperature, baryon chemical potential, baryon density and energy density.

4 Summary and conclusion

The production cross section around central rapidity for $\pi^{\pm}, K^{\pm}, p$ and $\bar{p}$ are observed in Pb+Pb collisions at CERN SPS. The temperature at freeze-out at Pb+Pb collisions is around 140 MeV. From comparison with hydrodynamical model calculation, the existence of transverse flow is suggested and the surface flow velocity β_s in Pb+Pb collisions ($\beta_s = 0.60 \pm 0.10$) is larger than S+S collisions ($\beta_s = 0.40 \pm 0.05$). At the CERN SPS energy, the strangeness chemical potential is close to 0. The baryon chemical potential is given from Pb+Pb collisions (184 ± 24 MeV) and larger than S+S collisions (147 ± 17 MeV). The baryon density, energy density at freeze-out are given from chemical potential and temperature. We get the baryon density and energy density by estimating the volume at formation time for S+S and Pb+Pb collisions at CERN SPS and Si+Pb at BNL AGS.

The CERN SPS data and BNL AGS data are different about the temperature and baryon density at freeze-out. On the other hand, the energy density at freeze-out in heavy ion collisions at SPS and AGS is almost same (60$\sim$70 MeV). The estimated energy density at formation time suggests that there is a possibility of QGP phase in Pb+Pb collisions at CERN SPS.

Acknowledgement

NA44 collaborators thanks for the staff at the CERN SPS accelerator complex and are grateful to the technical staff at CERN.

I would like to thank for colleagues of Hadron Physics laboratory and NA44 collaborators. Prof. O. Miyamura and Prof. T. Sugitate supported and gave me some suggestion. Dr. S. Esumi and Dr. N. Xu. give me some useful information about the way of analysis and discussed with me. Dr. H. Shiota and Dr. H. Ohnishi gave me many time of discussion from the point of view single particle analysis and 2 particle interferometer analysis, respectively.

Thanks, friends!

References

[1] H. Bøggild et al., *Phys. Lett.* **B302**, 510 (1993).

[2] N. Maeda,
Transverse momentum dependence of the space-time evolution of the particle source produced in S+Pb collisions at 200 GeV per nucleon, *to be submitted to the Department of Physics for a Doctor of Science Degree at the Hiroshima University*

[3] S. Esumi,
Collective Expansion in High-Energy Heavy-Ion Collisions at CERN SPS Energies, *submitted to the Department of Physics for a Doctor of Science Degree at the Hiroshima University*

[4] N. Maeda et al., *Nucl. Instr. and Meth.* **A346**, 132 (1994).

[5] E Schnedermann, J Sollfrank and U Heinz, *Phys. Rev.* **C48**, 2462 (1993).

[6] H. Shiota, *master thesis*,
Deuteron Production in Heavy-Ion Collisions at CERN SPS Energies.

[7] J. Sollfrank, M. Gaździcki, U. Heinz, J Rafelski, *Z. Phys.* **C61**, 659 (1994).

[8] P. Braun-Munzinger, J. Stachel, J. P. Wessels, N Xu, *Phys. Lett.* **B344**, 43 (1995).

[9] J. Letessier, J. Rafelski, A. Tounsi, *Phys. Lett.* **B328**, 499 (1994).

[10] H. R. Jaqaman, A. Z. Mekjian and J. Zamick, *Phys. Rev.* **C29**, 2067 (1984).

[11] J. Cleymans and H. Satz, *Z. Phys.* **C57**, 135 (1993).

[12] T. Csörgő and B. Lörstad,
CU-TP-717, hep-ph/9509213, LUNFD6/(NFFL-7082)-Rev. 1994

[13] B Müller, *Nucl. Phys.* **A590**, 3c (1995).

[14] T. Alber, *Nucl. Phys.* **A590**, 453c (1995).

[15] M. Gaździcki, *Nucl. Phys.* **A590**, 197c (1995).

[16] C. B. Dover, *Nucl. Phys.* **A590**, 333c (1995).

[17] J. Baechler et al., *Z. Phys.* **C58**, 367 (1993).

[18] K. Kadija, CHEP94 Ref. GLS0024